ISSN 1392–1207. MECHANIKA. 2015 Volume 21(2): 141–147

Digital true tooth surface modelling method of spiral bevel gear

Mo Shuai*, **Zhang Yidu****

**State Key Laboratory of Virtual Reality Technology and Systems, School of Mechanical Engineering & Automation, Beihang University, Beijing Engineering Technological Research Center of High-efficient & Green CNC Machining Process and Equipment, Beijing 100191, China, E-mail: moshuai2010@163.com*

***State Key Laboratory of Virtual Reality Technology and Systems, School of Mechanical Engineering & Automation, Beihang University, Beijing Engineering Technological Research Center of High-efficient & Green CNC Machining Process and Equipment, Beijing 100191, China, E-mail: ydzhang@buaa.edu.cn*

crossref http://dx.doi.org/10.5755/j01.mech.21.2.8397

1. Introduction

Spiral bevel gear have been found widely used in helicopter, truck transmissions and reducers for transformation of rotation and torque between intersected axes. Design of spiral bevel gear has been a topic of research by many scholars both in home and abroad. Obscure mathematical theory of spatial mesh of spiral bevel gear, complex machining method, and numerous parameters involved in machining processing, make it difficult to establish the precisely digital true tooth surface. So many papers only discussed standard spherical involute tooth surface. In order to study the CAM technology and CAE technology for stress analysis of spiral bevel gear, obtain the digital true tooth surface are much needed.

Many scholars all over the world have studied spiral bevel gear technology [1-14]. Their research methods for spiral bevel gear modeling can be concluded as the followed. Establish the equation of spherical involute based on geometric parameters of spiral bevel gear via mathematical methods, get the spherical involute curve via inputting equation into a CAD software or programming, and then scan or loft for the tooth surface [1-3]. Take advantage of ready-made commercial software, like the plug-in of UG to build spiral bevel gear, to automatically get the three-dimensional model by inputting basic parameters [4]. Obtain discrete point coordinates of tooth surface from Gleason Summary of Machine Settings, and then import them into a CAD software [5]. Calculate a set of coordinates of discrete points of the standard tooth surface through programming numerical values, and import those points into a CAD software for the tooth surface. These research results are of great significance under the given research phase.

In order to accurately grasp the effects of machining adjustment parameters on tooth surface error, tooth contact, and transmission error, it is an unavoidable task to seek a new method to model the true tooth surface. Modeling tooth surface with spherical involute, obviously treats the tooth surface as a standard involute tooth surface, taking for granted that all tooth surfaces are the same in view of the basic geometric parameters. As a matter of fact, the tooth surface of spiral bevel gears finally processed in practical industry, is anything but the absolutely standard spherical involute; and the tooth surface is only partial conjugate surface instead of absolutely conjugate surface. Tooth surfaces even with the same basic gear parameters can be different, since various factors contribute to their precise shapes. Contact area, transmission error and other design requirement will change tooth surfaces by adjusting machine adjustment parameters. Meanwhile, different designers will make various microscopic tooth surfaces, with different machine adjustment parameters, tooth contact forces, stress distributions and service lifespan. The former three methods failed to take machining adjustment parameters' effects on the microscopic tooth surface into consideration. Modeling through extracting discrete point coordinates of tooth surface from Gleason Summary of Machine Settings for a true tooth surface is indeed a big step forward, but it still could not get rid of the constraints of Gleason software, Gleason underlying algorithms and machine.

So the technology of true tooth surface precise modeling based on machining adjustment parameters becomes a pressing need. To study the effects of various machining adjustment parameters on tooth surface error and property of spiral bevel gear, precise tooth surfaces based on the given machining adjustment parameters are needed. The prerequisite to the contrastive study of theoretic tooth surface and error surface also lies in a precise and reliable tooth surface 3D model. Then, the machining adjustment parameters can be changed to gain the corresponding digitized true tooth surface, which can lay a solid basis for the subsequent finite element analysis of gear contact and transmission error analysis. Only in this way, are the conclusions from studies of instructive importance and reference value to practical production. Once the tooth surface model is not precise, all subsequent conclusions will become unhelpful and useless.

2. Mathematical model of gear tooth surface

2.1. Machine coordinate system of gear

The gear calculated in this paper is left hand (LH), and the cutter is mounted on the lower right of cradle during processing, so the cutter coordinate system is set in the lower right of cradle coordinate system as shown in Fig. 1. Subscript *2* in the coordinate system represents Gear, and Subscript *1* represents Pinion. Coordinate systems S_m, S_a, and S_b are fixed coordinate systems, rigidly connected to the machine. Coordinate systems S_2 and S_c are movable coordinate systems, rigidly connected to Gear and cradle. S_g is the cutter coordinate system of Gear, rigidly connected to S_c, the cradle coordinate system. As shown in Fig. 2, Ψ_c and Ψ_2 are the current angles of rotation of cradle and gear respectively. ΔE_m stands for blank offset, ΔX_B for sliding base, ΔX_D for machine center to back, S_r for radial setting, q for basic cradle angle, and γ_m for machine root angle.

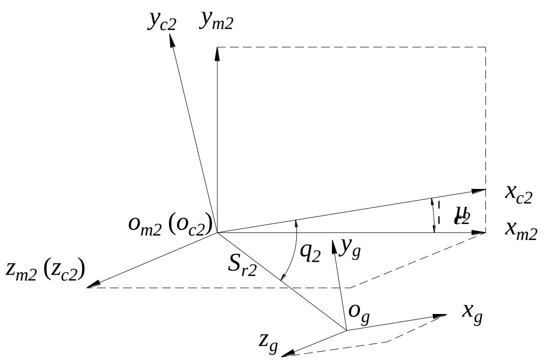

Fig. 1 Cradle coordinate system LH

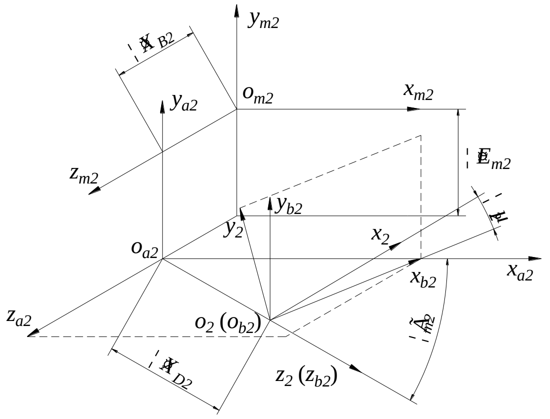

Fig. 2 Workpiece coordinate system

2.2. Equation of head-cutter surfaces

Gear is processed by generation method, using alternate blade cutter to simultaneously produce the convex side and concave side. When establishing the mathematical model of cutter, head-cutter is divided into two segments a and b as shown in Fig. 3. Segment a is the straight line part, while segment b is the fillet part. In the equations, the superscript of matrix in equation indicates the corresponding specific segment, and the subscript means the corresponding reference coordinate system. For example, Eq. (1) r_g is the vector function for cutter surfaces of segment a; Eq. (2) n_g is the normal vector for cutter surfaces of segment a; Eq. (3) r_g is the vector function for cutter surfaces of segment b; and Eq. (6) n_g is the normal vector for cutter surfaces of segment b. The meanings of scalar symbols X_ω, R_g, P_ω, α_g, R_g, R_μ, $P_{\omega 2}$ and λ_ω are explained in the corresponding figures and tables. Fig. 4 shows the generating tool cones for the concave side and convex side.

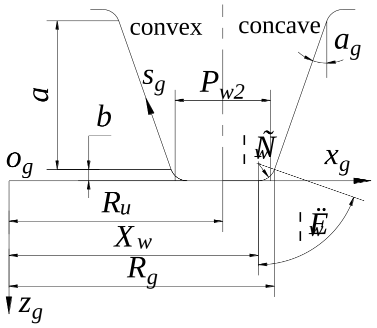

Fig. 3 The mathematical model of straight-line head-cutter

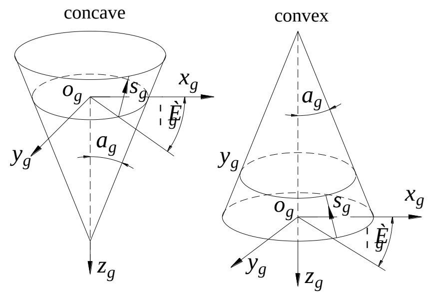

Fig. 4 Head-cutter coordinate system(straight-line)

$$r_g^{(a)}(s_g,\theta_g)=\begin{bmatrix}(R_g \pm s_g sin\alpha_g)cos\,\theta_g\\(R_g \pm s_g sin\alpha_g)sin\,\theta_g\\-s_g cos\alpha_g\end{bmatrix}, \tag{1}$$

$$n_g^{(a)}(\theta_g)=\begin{bmatrix}cos\,\alpha_g cos\,\theta_g\\cos\,\alpha_g sin\,\theta_g\\\pm sin\,\alpha_g\end{bmatrix}, \tag{2}$$

$$r_g^{(b)}(\lambda_\omega,\theta_g)=\begin{bmatrix}(X_\omega \pm \rho_\omega sin\,\lambda_\omega)cos\,\theta_g\\(X_\omega \pm \rho_\omega sin\,\lambda_\omega)sin\,\theta_g\\-\rho_\omega(1-cos\,\lambda_\omega)\end{bmatrix}, \tag{3}$$

$$X_\omega = R_g \mp \rho_\omega(1-sin\,\alpha_g)/\,cos\,\alpha_g\,, \tag{4}$$

$$R_g = R_u \pm \frac{P_{\omega 2}}{2}, \tag{5}$$

$$n_g^{(b)}(\theta_g)=\begin{bmatrix}sin\,\lambda_\omega cos\,\theta_g\\sin\,\lambda_\omega sin\,\theta_g\\\pm cos\,\lambda_\omega\end{bmatrix}. \tag{6}$$

The generating surfaces for the gear parabolic-profile head-cutter are formed by rotation of the blade about z_g of the head-cutter, θ_g is the rotation angle. The apex of the parabola is located at point M determined by parameter S_{g0}, called the parabola vertex location parameter, α_g is the

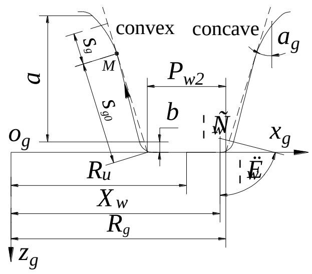

Fig. 5 The mathematical model of parabolic-profile head-cutter

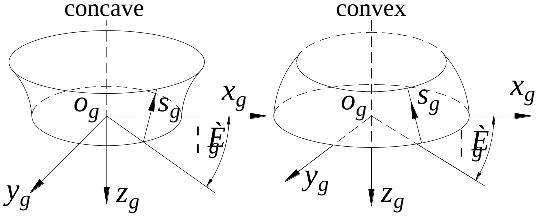

Fig. 6 Head-cutter coordinate system (parabolic-profile)

blade angle at point M, a_c is the parabola coefficient, ρ_w is the radius of circular arc profile of the fillet. In the case of grinding, the profiles shown in Fig. 5 represent the axial profiles of the grinder. Fig. 6 shows the generating surfaces of the parabolic-profile head-cutter.

$$r_g^{(a)}\left(s_g,\theta_g\right)=\begin{bmatrix}\left(R_g\pm\left(s_g+s_{g0}\right)sin\alpha_g\pm a_c s_g^2 cos\alpha_g\right)cos\theta_g\\ \left(R_g\pm\left(s_g+s_{g0}\right)sin\alpha_g\pm a_c s_g^2 cos\alpha_g\right)sin\theta_g\\ -\left(s_g+s_{g0}\right)cos\alpha_g+a_c s_g^2 sin\alpha_g\end{bmatrix}, \quad (7)$$

$$n_g^{(a)}\left(s_g,\theta_g\right)=\frac{\begin{bmatrix}\left(cos\alpha_g - 2a_c s_g sin\alpha_g\right)cos\theta_g\\ \left(cos\alpha_g - 2a_c s_g sin\alpha_g\right)sin\theta_g\\ \pm sin\alpha_g \pm 2a_c s_g cos\alpha_g\end{bmatrix}}{\sqrt{1+4a_c^2 s_g^2}}, \quad (8)$$

$$r_g^{(b)}\left(\lambda_\omega,\theta_g\right)=\begin{bmatrix}\left(X_\omega\pm\rho_\omega\, sin\,\lambda_\omega\right)cos\,\theta_g\\ \left(X_\omega\pm\rho_\omega\, sin\,\lambda_\omega\right)sin\,\theta_g\\ -\rho_\omega\left(1-cos\,\lambda_\omega\right)\end{bmatrix}, \quad (9)$$

$$n_g^{(b)}\left(\lambda_\omega,\theta_g\right)=\begin{bmatrix}sin\,\lambda_\omega\, cos\,\theta_g\\ sin\,\lambda_\omega\, sin\,\theta_g\\ \pm cos\,\lambda_\omega\end{bmatrix}, \quad (10)$$

Eq. (7) r_g is the vector function for parabolic-profile cutter surfaces of segment a; Eq. (8) n_g is the normal vector for parabolic-profile cutter surfaces of segment a; Eq. (9) r_g is the vector function for parabolic-profile cutter surfaces of segment b; and Eq. (10) n_g is the normal vector for parabolic-profile cutter surfaces of segment b. The geometrical significance of same scalar symbols in matrix can be found in Fig. 3 to Fig. 6.

2.3. Equation of gear tooth surface

Superscript of matrix in equation indicates the corresponding specific segment; subscript indicates the corresponding reference coordinate system; and the symbol in the bracket indicates the variable. For instance, M_{2g} matrix represents the coordinates transferring from S_g to S_2. Other transformational matrix share the similar meaning. Eqs. (11) and (20) are the vector function transferring from cutter coordinate system to gear coordinate system for segment a and b. Eqs. (18) and (21) refer to the mesh conditions for Gear tooth surface of segment a and b. Eqs. (19) and (22) mean the vector equation for gear tooth surface of segment a and b:

$$r_2^{(a)}\left(s_g,\theta_g,\psi_2\right)=M_{2g}\left(\psi_2\right)r_g^{(a)}\left(s_g,\theta_g\right), \quad (11)$$

$$M_{2g}\left(\psi_2\right)=M_{2b2}M_{b2a2}M_{a2m2}M_{m2c2}M_{c2g}, \quad (12)$$

$$M_{c2g}=\begin{bmatrix}1&0&0&S_{r2}\,cos\,q_2\\0&1&0&S_{r2}\,sin\,q_2\\0&0&1&0\\0&0&0&1\end{bmatrix}, \quad (13)$$

$$M_{m2c2}=\begin{bmatrix}cos\,\psi_{c2}&-sin\psi_{c2}&0&0\\sin\psi_{c2}&cos\,\psi_{c2}&0&0\\0&0&1&0\\0&0&0&1\end{bmatrix}, \quad (14)$$

$$M_{a2m2}=\begin{bmatrix}1&0&0&0\\0&1&0&\Delta E_{m2}\\0&0&1&-\Delta X_{B2}\\0&0&0&1\end{bmatrix}, \quad (15)$$

$$M_{b2a2}=\begin{bmatrix}sin\,\gamma_{m2}&0&-cos\,\gamma_{m2}&0\\0&1&0&0\\cos\,\gamma_{m2}&0&sin\,\gamma_{m2}&-\Delta X_{D2}\\0&0&0&1\end{bmatrix}, \quad (16)$$

$$M_{2b2}=\begin{bmatrix}cos\,\psi_{c2}&sin\psi_{c2}&0&0\\-sin\psi_{c2}&cos\,\psi_{c2}&0&0\\0&0&1&0\\0&0&0&1\end{bmatrix}, \quad (17)$$

$$\left(\frac{\partial r_2^{(a)}}{\partial s_g}\frac{\partial r_2^{(a)}}{\partial\theta_g}\right)\frac{\partial r_2^{(a)}}{\partial\psi_2}=f_{2g}^{(a)}\left(s_g,\theta_g,\psi_2\right)=0, \quad (18)$$

$$R_2^{(a)}\left(\theta_g,\psi_2\right)=r_2^{(a)}\left(s_g\left(\theta_g,\psi_2\right),\theta_g,\psi_2\right), \quad (19)$$

$$r_2^{(b)}\left(\lambda_\omega,\theta_g,\psi_2\right)=M_{2g}\left(\psi_2\right)r_g^{(b)}\left(\lambda_\omega,\theta_g\right), \quad (20)$$

$$\left(\frac{\partial r_2^{(b)}}{\partial\lambda_\omega}\frac{\partial r_2^{(b)}}{\partial\theta_g}\right)\frac{\partial r_2^{(b)}}{\partial\psi_2}=f_{2g}^{(b)}\left(\lambda_\omega,\theta_g,\psi_2\right)=0, \quad (21)$$

$$R_2^{(b)}\left(\theta_g,\psi_2\right)=r_2^{(b)}\left(\lambda_\omega\left(\theta_g,\psi_2\right),\theta_g,\psi_2\right). \quad (22)$$

3. Mathematical model of pinion tooth surface

3.1. Machine coordinate system of pinion

Pinion is processed by the method of modified roll, using the inside and outside blade cutters to process the concave and convex sides of tooth surface. Pinion is RH, and the cutter is mounted on the upper right of cradle, so the cutter coordinate system is set in the upper right of cradle coordinate system as shown in Figs. 7 and 8. Subscript 1 in coordinate system represents pinion. Subscript p represents cutter for pinion. Other symbols share the similar definitions with those of gear.

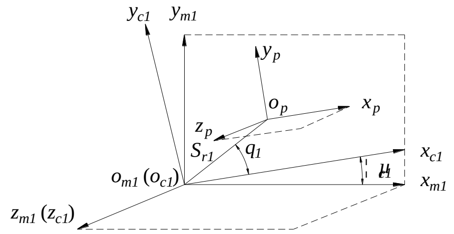

Fig. 7 Cradle coordinate system RH

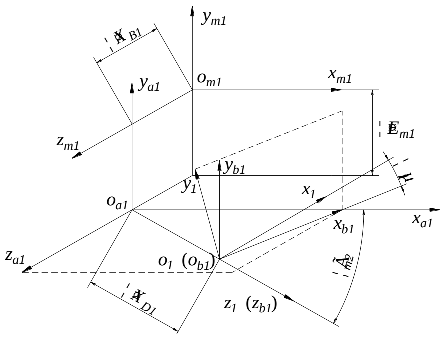

Fig. 8 Workpiece coordinate system

3.2. Equation of head-cutter surfaces

Both the inside and outside cutters are used in the processing of pinion, and the mathematical model for cutter is established as shown in Figs. 9 and 10.

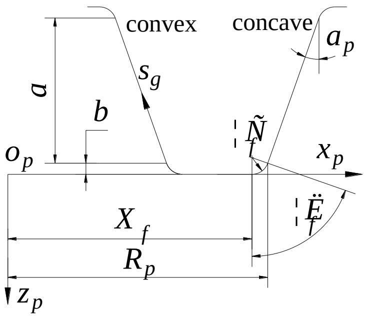

Fig. 9 The mathematical model of straight-line head-cutter

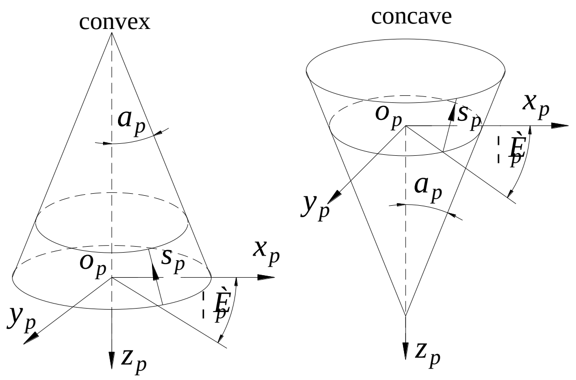

Fig. 10 Head-cutter coordinate system

$$r_p^{(a)}\left(s_p,\theta_p\right)=\begin{bmatrix}\left(R_p\mp s_p sin\,\alpha_p\right)cos\,\theta_p\\ \left(R_p\pm s_p sin\,\alpha_p\right)sin\,\theta_p\\ -s_p\,cos\,\alpha_p\end{bmatrix}, \tag{23}$$

$$n_p^{(a)}\left(\theta_p\right)=\begin{bmatrix}cos\,\alpha_p\,cos\,\theta_p\\ cos\,\alpha_p\,sin\,\theta_p\\ \mp sin\,\alpha_p\end{bmatrix}, \tag{24}$$

$$r_p^{(b)}\left(\lambda_f,\theta_p\right)=\begin{bmatrix}\left(X_f\mp\rho_f\,sin\,\lambda_f\right)cos\,\theta_p\\ \left(X_f\mp\rho_f\,sin\,\lambda_f\right)sin\,\theta_p\\ -\rho_f\left(1-cos\,\lambda_f\right)\end{bmatrix}, \tag{25}$$

$$n_p^{(b)}\left(\theta_p\right)=\begin{bmatrix}sin\,\lambda_f\,cos\,\theta_p\\ sin\,\lambda_f\,sin\,\theta_p\\ \mp cos\,\lambda_p\end{bmatrix}. \tag{26}$$

3.3. Equation of pinion tooth surface

Eqs. (27) and (28) are the vector function transferring from cutter coordinate system to pinion coordinate system for segment a and b. Eqs. (42) and (43) are the meshing equations of pinion for segment a and b, v_{m1} is the relative velocity between workpiece (pinion) and cutter at coordinate system S_{m1}.

$$r_1^{(a)}\left(s_p,\theta_p,\psi_1\right)=M_{1p}\left(\psi_{c1}\right)r_p^{(a)}\left(s_p,\theta_p\right), \tag{27}$$

$$r_1^{(b)}\left(s_f,\theta_p,\psi_{c1}\right)=M_{1p}\left(\psi_{c1}\right)r_p^{(b)}\left(s_f,\theta_p\right), \qquad 28)$$

$$M_{1p}\left(\psi_{c1}\right)=M_{1b1}M_{b1a1}M_{a1m1}M_{m1c1}M_{c1p}\,, \tag{29}$$

$$M_{c1p}=\begin{bmatrix}1&0&0&S_{r_1}\,cos\,q_1\\0&1&0&S_{r_1}\,sin\,q_1\\0&0&1&0\\0&0&0&1\end{bmatrix}, \tag{30}$$

$$M_{m1c1}=\begin{bmatrix}cos\,\psi_{c1}&-sin\,\psi_{c1}&0&0\\sin\,\psi_{c1}&cos\,\psi_{c1}&0&0\\0&0&1&0\\0&0&0&1\end{bmatrix}, \tag{31}$$

$$M_{a1m1}=\begin{bmatrix}1&0&0&0\\0&1&0&\Delta E_{m1}\\0&0&1&-\Delta X_{B1}\\0&0&0&1\end{bmatrix}, \tag{32}$$

$$M_{b1a1}=\begin{bmatrix}sin\,\gamma_{m1}&0&-cos\,\gamma_{m1}&0\\0&1&0&0\\cos\,\gamma_{m1}&0&sin\,\gamma_{m1}&-\Delta X_{D1}\\0&0&0&1\end{bmatrix}, \tag{33}$$

$$M_{1b1}=\begin{bmatrix}cos\,\psi_1&sin\,\psi_1&0&0\\-sin\,\psi_1&cos\,\psi_1&0&0\\0&0&1&0\\0&0&0&1\end{bmatrix}, \tag{34}$$

$$\psi_1=m_{1c}\left(\psi_{1c}-C\psi_{c1}^2-D\psi_{c1}^3\right), \tag{35}$$

$$v_{m1}^{(a)}=\left[\left(\omega_{m1}^{(p)}-\omega_{m1}^{(1)}\right)\times r_{m1}\right]-\left(\overline{o_{m1}o_{a1}}\times\omega_{m1}^{(1)}\right), \tag{36}$$

$$r_{m1}=M_{m1c1}M_{c1p}r_p^{(a)}\left(s_p,\theta_p\right), \tag{37}$$

$$\overline{o_{m1}o_{a1}}=\left[0\quad-\Delta E_{m1}\quad\Delta X_{B1}\right]^T, \tag{38}$$

$$\omega_{m1}^{(1)} = \left[cos\,\gamma_{m1} \quad 0 \quad sin\,\gamma_{m1} \right]^T, \tag{39}$$

$$\omega_{m1}^{(p)} = \left[0 \quad 0 \quad m_{1c}\left(\psi_{c1}\right) \right]^T, \tag{40}$$

$$m_{1c}\left(\psi_{c1}\right) = \frac{1}{m_{1c}\left(1 - 2C\psi_{c1} - 3D\psi_{c1}^2\right)}, \tag{41}$$

$$n_{m1}^{(a)} v_{m1}^{(a)} = f_{1p}^{(a)}\left(s_p, \theta_p, \psi_{c1}\right) = 0, \tag{42}$$

$$n_{m1}^{(b)} v_{m1}^{(b)} = f_{1p}^{(b)}\left(\lambda_f, \theta_p, \psi_{c1}\right) = 0. \tag{43}$$

4. Machining adjustment parameters calculation

Gear is processed by generation method with alternate blade cutter, while pinion is processed with two cutters, each processing one side of the tooth. According to spatial mesh theory, program the mathematical principle of the construction of the tooth surface of the above gear and pinion, and solve the nonlinear equations. Make use of Matlab to program and calculate the machining adjustment parameters of gear and pinion, then put in the above parameters to get their tooth surface discrete point clouds. Fig. 11 is the technology roadmap of tooth surface modeling, Table 1 is design parameters of gear set; Tables 2 and 3 are the calculated adjusting parameters for gear and pinion respectively.

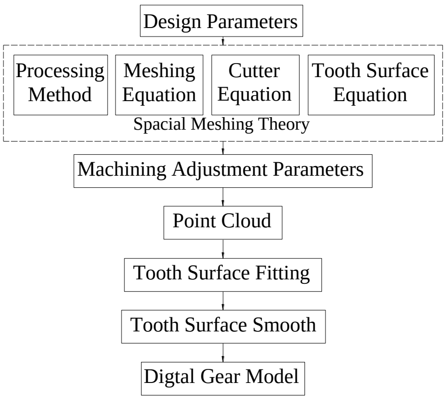

Fig. 11 Technology roadmap of tooth surface modeling

Table 1

Design parameters of gear set

Parameters	Pinion	Gear
Number of teeth	9	33
Module, mm	4.838	4.838
Shaft angle,°	90.0	90.0
Pressure angle,°	22.0	22.0
Hand of spiral	RH	LH
Mean spiral angle,°	32.0	32.0
Face width, mm	27.5	27.5
Pitch angles,°	15.2551	74.7449
Root angles,°	13.8833	69.5833
Face angles,°	20.4167	76.1167
Addendum, mm	6.64	1.76
Dedendum, mm	2.79	7.67
Clearance, mm	1.03	1.03

Table 2

Machining adjustment parameters of gear

Parameters	Convex	Concave
Cutter radius R_μ, mm	63.5	63.5
Blade angle α_g,°	-22.0	-22.0
Point width $P_{\omega 2}$, mm	2.54	2.54
Root filler radius ρ_ω, mm	1.524	1.524
Radial distance S_{r2}, mm	64.3718	64.3718
Cradle angle q_2 (°)	-56.78	-56.78
Blank offset $\varDelta E_{m2}$ (mm)	0	0
Sliding base $\varDelta X_{B2}$ (mm)	-0.2071	-0.2071
Machine center to back $\varDelta X_{D2}$	0	0
Machine root angle γ_{m2},°	69.5833	69.5833
Velocity ratio m_{2c2}	1.032331	1.032331

Table 3

Machining adjustment parameters of pinion

Parameters	Convex	Concave
Cutter radius R_p, mm	69.7529	59.9195
Blade angle α_p, °	-22.0	22.0
Root filler radius ρ_f, mm	0.635	0.635
Radial distance S_{r1}, mm	66.0406	62.7677
Cradle angle q_1,°	52.8382	59.4386
Blank offset $\varDelta E_{m1}$, mm	-3.4163	4.4841
Sliding base $\varDelta X_{B1}$, mm	-1.0519	-0.2013
Machine center to back $\varDelta X_{D1}$	1.0079	-2.5371
Machine root angle γ_{m1},°	13.8833	13.8833
Velocity ratio m_{1c}	3.8726	3.6963
Modified roll coefficient C	0.00175	-0.002
Modified roll coefficient D	-0.01	-0.007

5. Digital true tooth surface modeling

Fig. 12 to Fig. 15 are the process of point cloud data input to software, Figs. 16 and 17 are the process of tooth surface modeling. The curved surface reconstructed in the 3D software via leading point cloud documents by means of reverse engineering, is not smooth but stitched by many small curved surfaces, as shown in Figs. 18 and 19. A crack seems to be in the middle of the curved surface, which not only influences the visual effects, but also prevents contact analysis and solution in FEA, and even contact setting. Therefore, it’s necessary to adopt other methods or approaches to deal with the reconstruction. The digitized and high-precision true tooth surfaces under the study of this paper are shown in Figs. 20 and 21.

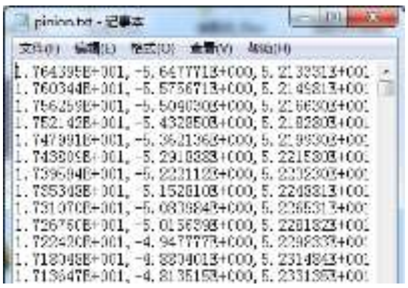

Fig. 12 Point cloud data file for pinion

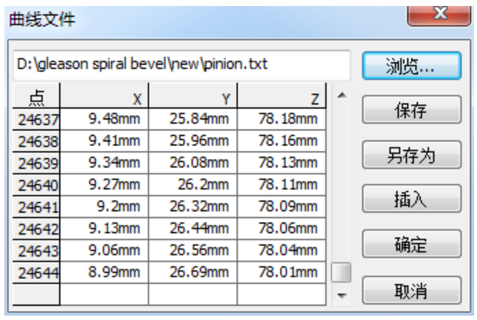

Fig. 13 Input point cloud data for tooth surface of pinion

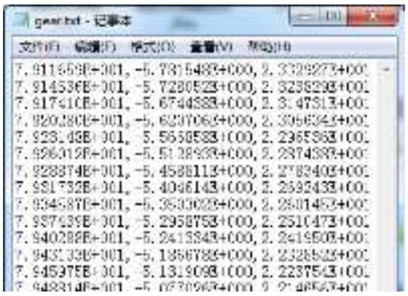

Fig. 14 Point cloud data file for gear

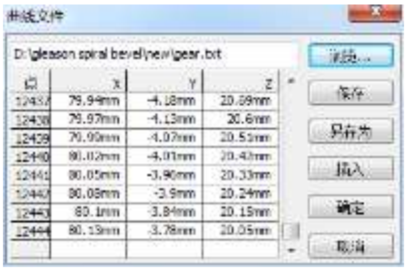

Fig. 15 Input point cloud data for tooth surface of gear

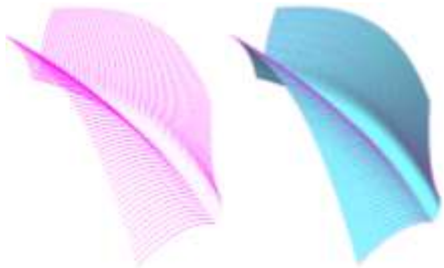

Fig. 16 Point cloud data and tooth surface of pinion

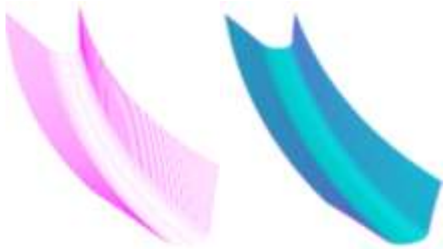

Fig. 17 Point cloud data and tooth surface of gear

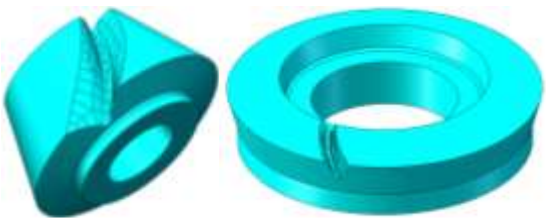

Fig. 18 The uneven tooth surface (one tooth)

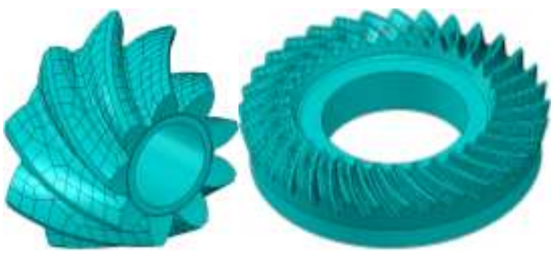

Fig. 19 The uneven tooth surface of gear and pinion

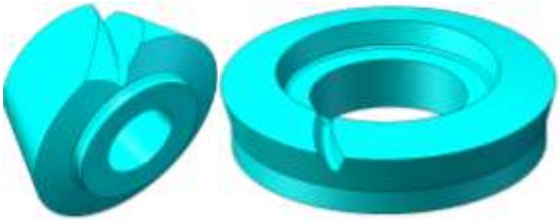

Fig. 20 The smooth tooth surface (one tooth)

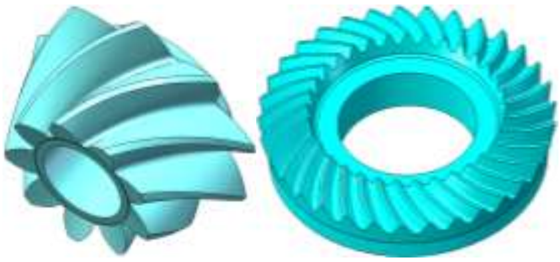

Fig. 21 The smooth tooth surface of gear and pinion

6. Gear cutting experiment

To verify the technical advancement and practicability in engineering digitized true tooth surface of spiral bevel gear based on machining adjustment parameters, this study, gets the NC codes via NC process simulation software from 3D model with machining adjustment parameters and then inputs the codes to five-axis NC machine tools to conduct gear cutting experiments. Gear cutting experiment is made in YH606 CNC Curved Tooth Bevel Gear Generator made in China. The gear and pinion after processing are as shown in Fig. 22.

Fig. 22 The processed pinion and gear

7. Conclusion

According to the spatial meshing theory, both the machining adjustment parameters of gear and pinion, and the discrete point clouds of tooth surface based on machining adjustment parameters have been calculated through programming. By establishing digitized and high-precision true tooth surface of spiral bevel gear, and conducting the gear cutting processing experiments on the five-axis NC machine tools, the advancement and practicability of spiral bevel gear true tooth surface precise modeling based on machining adjustment parameters have been verified, which lays a solid foundation for tooth loading contact analysis of the digitized true tooth surface and design of non-standard spiral bevel gear in the future.

Acknowledgment

This thesis is supported by Aeronautical Science Foundation of China (Grant No. 20130451010), National Science, Technology Major Project(Grant No. 2013ZX040 01061), National Key Technology Support Program(Grant No. 2014BAF08B01), Beijing Engineering Technological Research Center of High-efficient & Green CNC Machining Process and Equipment funded programs (Grant No.Z141104004414067), and the Innovation Foundation of BUAA for PhD Graduates. Thanks also go to Dr. Wang Peng for his constant assistance in the course of the research.

References

1. **Yang, Yanni.** 2009. Dynamic Analysis and Optimization of Spiral Bevel Gear System, Chongqing, Chin: Chongqing University (in Chinese).
2. **Hong, Zhaobin.** 2013. New Milling Method of Spiral Bevel Gear Based on Generating Principle of Tooth Surface with Spherical Involute, Changchun, China: Jilin University (in Chinese).
3. **Wang, Ben; Hua, Lin.** 2011. Dynamic modal analysis of automotive spiral bevel gears with high rotation speed, Automotive Engineering 33(5): 447-448 (in Chinese).
4. **Yao, Ting-qiang; Wang, Li-hua; Tan Yang.** 2012. Contact dynamics analysis of spiral bevel gear, Journal of Vibration and Shock 31(9): 128-130 (in Chinese).
5. **Li, Yuan.** 2005. A Simulating Analysis for Spiral Bevel Gear Meshing in Aerostat Reducer, Changsha, China, National University of Defense Technology (in Chinese).
6. **Wang, Peng.** 2013. Global Synthesis for Face Milled Spiral Bevel Gears with Zero Transmission Errors, Beijing, China: Beihang University (in Chinese).
7. **Julien, Astoul; Jérôme, Geneix; Emmanuel, Mermoz**. 2013. A simple and robust method for spiral bevel gear generation, International Journal for Interactive Design and Manufacturing 7(1): 37-49. http://dx.doi.org/10.1007/s12008-012-0163-y.
8. **Faydor, L. Litvin; Alfonso, Fuentes; Qi, Fan; Robert, F. Handschuh.** 2002. Computerized design, simulation of meshing, and contact and stress analysis of face-milled formate generated spiral bevel gears, Mechanism and Machine Theory 37(5): 441-459. http://dx.doi.org/ 10.1016/S0094-114X(01)00086-6.
9. **John, Argyris; Alfonso, Fuentes; Faydor, L. Litvin.** 2002. Computerized integrated approach for design and stress anaysis of spiral bevel gears, Mechanism and Machine Theory 191(11): 1057-1095. http://dx.doi.org/10.1016/S0045-7825(01)00316-4.
10. **Ignacio, Gonzalez-Perez; Alfonso, Fuentes; Kenichi, Hayasaka.** 2010. Analytical determination of basic machine-tool settings for generation of spiral bevel gears from blank data, Journal of Mechanical Design, 132(10): 1-11. http://dx.doi.org/10.1115/1.4002165.
11. **Joe¨l Teixeira, Alves; Miche`le, Guingand; Jean-Pierre de Vaujany.** 2013. Designing and manufacturing spiral bevel gears using 5-axis computer numerical control (CNC) milling machines, Journal of Mechanical Design 135(2): 1-6. http://dx.doi.org/10.1115/1.4023153.
12. **Qi, Fan.** 2011. Optimization of face cone element for spiral bevel and hypoid gears, Journal of Mechanical Design 133(9): 1-7. http://dx.doi.org/10.1115/1.4004546.
13. **Lee, H.W.; Lee, K.O.; Chung, D.H.** 2010. A kinematic investigation of a spherical involute bevel-geared system, Journal of Mechanical Engineering Science 224(6): 1335-1348. http://dx.doi.org/10.1243/09544062JMES1624.
14. **Simon, Vilmos V.** 2009. Design and manufacture of spiral bevel gears with reduced transmission errors, Journal of Mechanical Design 131(4): 1-11. http://dx.doi.org/10.1115/1.3087540.

Mo Shuai, Zhang Yidu

DIGITAL TRUE TOOTH SURFACE MODELLING METHOD OF SPIRAL BEVEL GEAR

S u m m a r y

A method for digital true gear tooth surfaces of spiral bevel gear is presented based on the meshing theory of gear and conjugate surface. The microscopic true tooth surface varies according to different machining adjustment parameters, so the true tooth surface of spiral bevel gear is not standard spherical involute. The study Obtained the discrete points on the digital true surface from solving equation set based on meshing theory and successfully established a spiral bevel gear geometry model. The developed method verified by the machining adjustment parameters in engineering and precisely digital spiral bevel gear model. The study put forward a new method for the spiral bevel gear machining of non-standard digital true gear tooth surfaces, breaking the limitations of conventional modeling method based on stand spherical involute. Obtained a precisely digitized true tooth surface of spiral bevel gear based on machining adjustment parameters, which will have great value for transmission error analysis and true tooth contact analysis.

Keywords: digital tooth surface, spiral bevel gear, modeling method.

Received October 15, 2014
Accepted March 12, 2015